Catalysis Letters Vol. 103, Nos. 3–4, October 2005 (© 2005)
DOI: 10.1007/s10562-005-7163-5

XAFS characterization of Pt–Fe/zeolite catalysts for preferential oxidation of CO in hydrogen fuel gases

Masashi Kotobuki[a], Takafumi Shido[b], Mizuki Tada[b], Hiroyuki Uchida[a], Hisao Yamashita[c], Yasuhiro Iwasawa[b], and Masahiro Watanabe[c,*]

[a]*Graduate School of Engineering, University of Yamanashi, Takeda 4, Kofu, 400-8510, Japan*
[b]*Department of Chemistry, Graduate School of Science, The University of Tokyo, 7-3-1 Hongo, Bunkyo-ku, 113-0033, Japan*
[c]*Clean Energy Research Center, University of Yamanashi, Takeda 4, Kofu, 400-8510, Japan*

Received 25 February 2005; accepted 2 June 2005

We have developed a new Pt–Fe/mordenite (Pt–Fe/M) catalyst which shows remarkably high activity and selectivity for the oxidation of CO in H_2-rich gas compared with Pt/M. In the present work, to understand the role and structure of Pt and Fe in the Pt–Fe/M catalyst, the states of metallic components in ion-exchanged, H_2 pre-treated and post-PROX (preferential oxidation of CO) samples have been studied by means of XAFS. It was confirmed that Pt forms the metallic clusters after H_2 pretreatment or the PROX experiment, whereas a large part of Fe exists as oxides even after the H_2 treatment. At post-analysis of the catalysts used for the PROX experiment, an increase in coordination number of Fe–O was observed. Pt clusters in the Pt–Fe(2:1 weight ratio)/M catalyst, which showed the highest PROX performance, were found to have a different electronic structure from the other catalysts. Additionally, preferential CO adsorption onto Pt sites at Pt–Fe/M was clearly demonstrated by infrared spectroscopy analysis in a stream of 1% CO containing H_2. Based on these results, the superior PROX mechanism was discussed.

KEY WORDS: Pt–Fe catalyst; mordenite catalyst; preferential oxidation of carbon monoxide; selective oxidation of carbon monoxide; fuel cell; XAFS.

1. Introduction

Polymer electrolyte fuel cells (PEFCs) are attracting much attention as power sources in electric vehicles (EV) and residential power sources. The residential PEFCs are operated with reformed gases from natural gas, LPG or kerosene. However, a conventional Pt anode catalyst operating with reformed gases is seriously poisoned by a small amount of CO [1]. We showed that the CO concentration acceptable for the operations is < 10 ppm at Pt anode [2] and ≤ 100 ppm at CO-tolerant Pt alloy anodes [3], whereas the concentration of CO in reformates is about 1% in general. The removal of CO is also essential for the EV PEFC operation, where high purity H_2 is required.

PROX (preferential oxidation of CO) process on catalysts is one of the choices to achieve it. Noble metal catalysts supported on some oxides [4] or carbon [5] have been reported for that purpose so far. We have proposed Pt catalysts supported on zeolites for the removal of 1% CO from H_2-rich gas by the PROX, taking advantage of its "chemical and molecular sieve effect" [6–8]. In our latest work [9], an addition of Fe to Pt/mordenite catalyst shows better PROX performance than Pt/mordenite. Especially, we found 4 wt% Pt–2 wt% Fe/mordenite exhibits the best performance in various composition catalysts, i.e. 100% of CO conversion and CO selectivity just by the addition of stoichiometric amounts of O_2 between 80 and 200 °C. In this paper, we report the results of XAFS analysis on the Pt–Fe/mordenite catalysts and discuss about the distinctive properties.

2. Experimental

Pt and Fe were supported on a reference mordenite sample (supplied by the Catalysis Society of Japan) by a conventional ion-exchange method [6–9]. The ratios Pt/Fe were 3:1, 2:1, and 1:1 in wt%, while Fe loading was constant at 2 wt%. After drying in vacuum, they were sieved to obtain 100–200 mesh fractions. The sample is denoted as an "ion-exchanged" catalyst.

XAFS experiments at Pt L_{III} edge and Fe K edge were performed in a transmission mode at room temperature at BL-9A station in Photon Factory (PF, Tsukuba, Japan). Pt foil, PtO_2, Fe foil, FeO, and Fe_2O_3 were used as reference samples. Fe K edge and Pt L_{III} edge calibrations of the beamline were performed by measuring the edge positions of Fe and Pt foil, respectively. Each sample was loaded in a specially designed glass cell, which enables XAFS measurement of the sample treated under various atmospheres without exposing air. The glass cell has two stopcocks at the

* To whom correspondence should be addressed.

ends. First, the sample placed in the glass cell was oxidized in an O_2 flow at 500 °C for 1 h and then reduced in a H_2 flow at 500 °C for 1 h. After cooling quickly to room temperature in H_2 flow, both stopcocks were closed to seal the cell filled with H_2 gas. Then, XAFS spectra of the samples were measured. It is denoted as "H_2 pre-treated" catalyst.

The H_2 pre-treated sample was subsequently treated in a flow of gas mixture containing 1% CO, 0.5% O_2, and H_2 balance at 200 °C for 1 h, followed by cooling to room temperature in the same gas flow. The sample thus treated is denoted as "post-PROX" catalyst. Then, the post-PROX samples were performed XAFS measurements.

Fe K edge and Pt L_{III} edge EXAFS spectra were extracted from XAS data by using Autobk [10] so that oscillations whose wavelength less than 1 $Å^{-1}$ was filtered out. k^3-weighted EXAFS functions were Fourier transformed to R-space and fitted in R-space by Fe–Fe, Fe–Pt, and Fe–O contributions for Fe K edge and Pt–N, Pt–Pt, and Pt–Fe contributions for Pt L_{III} edge. Fitting to the Fe K and Pt L_{III} edge data of Pt–Fe(2:1)/M was performed simultaneously. The Fourier filtering k-range and fitting R-ranges were shown in tables 1 and 2. Above Fourier filtering and curve fitting were preformed by using Feffit program [11].

The fitting parameters are coordination number, inter-atomic distance, and Debye–Waller factor for each shell, and correction of threshold energy (E_0). Phase shifts and backscattering amplitudes used in the fittings were calculated theoretically by using Feff8 [12]. Coefficients of multi photon effect ($S_0^2 = 1$) were obtained experimentally by analyzing EXAFS data of reference compounds. Residual factor was calculated by using the following formula.

$$R_f(\%) = \frac{\sum_{i=1}^{N}\left\{[\mathrm{Re}(\mathrm{f}_i)]^2 + [\mathrm{Im}(\mathrm{f}_i)]^2\right\}}{\sum_{i=1}^{N}\left\{[\mathrm{Re}(\tilde{\chi}_{\mathrm{data}i})]^2 + [\mathrm{Im}(\tilde{\chi}_i)]^2\right\}} \times 100$$

A thermogravimetry of ion-exchanged catalyst was performed using TG–DTA (MAC science TG-DTA 2000) connected to a mass spectrometer (MAC science Thermolab). A small amount of sample (ca. 10 mg) was heated from room temperature to 700 °C at heating rate of 10 °C/min in flowing Ar.

Fourier transform infrared spectroscopy (FTIR) measurement was performed by using FTIR-500 with a diffused reflectance attachment (JASCO) available to control the temperature. Pt–Fe(2:1)/M sample was placed in the attachment and pre-treated to obtain the sample similar to "H_2 pre-treated" mentioned above. After the treatment, the IR spectra was taken in a flow of reactant–gas mixture (1% CO and H_2 balance) and then in N_2 atmosphere at 30 or 200 °C.

3. Results and discussion

3.1. TG–MS analyses

TG–MS profiles of ion-exchanged Pt–Fe(2:1)/M (4 wt% Pt loading) are shown in figure 1. Two step weight losses are observed in TG curve at 50–200 °C and 400–600 °C. From the MS profiles simultaneously recorded, the weight losses at low and high temperatures were ascribed to H_2O ($m/z = 18$) and NH_3 ($m/z = 17$), respectively. The observed weight loss corresponding to NH_3 is 1.6 wt%, that is well consistent with the calculated value, 1.4 wt%, supposing that Pt was supported on mordenite as $Pt(NH_3)_4$. Similar result was obtained

Table 1
Results of EXAFS analysis on Pt–Fe(2:1)/M in different treatment stages

	Center atom	Scatter	N	R (Å)	σ^2 (Å$\times 10^{-3}$)	ΔE (eV)	R_f (%)	k range[d] ($Å^{-1}$)	R range[e](Å)
Ion-exchanged[a]	Pt	N	3.9 ± 0.3	2.03 ± 0.005	2.56 ± 0.60	2.8 ± 0.9	1.4	3–12	1.0–3.0
	Fe	Fe	4.7 ± 0.2	3.00 ± 0.02	19.87 ± 6.33	−1.4 ± 1.6	1.3	3–10	1.0–3.0
		O	5.0 ± 0.1	1.97 ± 0.01	12.54 ± 2.15				
H_2 pre-treated[b]	Pt	Pt	2.1 ± 0.1	2.70 ± 0.01	2.33 ± 3.17	1.6	2.6	3–12	1.0–3.0
		Fe	4.6 ± 0.4	2.58 ± 0.01	14.07 ± 3.15				
	Fe	Pt	2.9 ± 2.0	2.58 ± 0.01	14.07 ± 3.15	−7.1		3–10	1.0–3.0
		Fe	2.0 ± 1.5	2.48 ± 0.10	18.83 ± 5.18				
		O	2.6 ± 1.0	2.06 ± 0.06	10.96 ± 20.08				
Post-PROX[c]	Pt	Pt	6.4 ± 0.1	2.74 ± 0.002	8.43 ± 0.62	4.5 ± 0.4	0.3	3–12	1.9–3.0
		Fe	1.9 ± 0.1	2.62 ± 0.003	9.09 ± 0.75				
	Fe	Pt	2.3 ± 0.1	2.62 ± 0.003	9.09 ± 0.75	−6.3 ± 1.4		3–9	1.0–3.0
		Fe	–	–	–				
		O	4.3 ± 0.2	2.00 ± 0.02	18.05 ± 3.42				

[a]Pre-cursors of Pt and Fe catalysts loaded by ion-exchanging method, followed by vacuum evacuation.
[b]In H_2 flow for 1 h after O_2 flow for 1 h at 500 °C.
[c]Under 1%CO, 0.5%O_2, H_2 balance flow for 1 h at 200 °C.
[d]k range for Fourier transformation.
[e]Fitting range in R-space.

Table 2
EXAFS analysis results on Pt center atom in Pt–Fe/M (Pt/Fe = 3:1, 2:1, 1:1)

	Treatment	Scatter	N	R (Å)	σ^2 (Å$\times 10^{-3}$)	ΔE (eV)	R_f (%)	k range[c] (Å^{-1})	R range[d](Å)
Pt–Fe(3:1)/M	H_2 pre-treated[a]	Pt	6.5 ± 0.1	2.72 ± 0.01	7.23 ± 0.54	3.4 ± 0.8	0.4	3–17	1.8–3.1
		Fe	2.2 ± 0.1	2.63 ± 0.01	10.23 ± 1.83				
	Post-PROX[b]	Pt	6.2 ± 0.1	2.72 ± 0.01	6.69 ± 0.48	4.2 ± 0.9	0.1	3–17	1.8–3.1
		Fe	2.4 ± 0.1	2.67 ± 0.01	10.45 ± 1.69				
Pt–Fe(2:1)/M	H_2 pre-treated	Pt	2.1 ± 0.1	2.70 ± 0.01	2.33 ± 3.17	1.6	2.6	3–12	1.0–3.0
		Fe	4.6 ± 0.4	2.58 ± 0.01	14.07 ± 3.15				
	Post-PROX	Pt	6.4 ± 0.1	2.74 ± 0.002	8.43 ± 0.62	4.5 ± 0.4	0.3	3–12	1.9–3.0
		Fe	1.9 ± 0.1	2.62 ± 0.003	9.09 ± 0.75				
Pt–Fe(1:1)/M	H_2 pre-treated	Pt	2.5 ± 0.1	2.71 ± 0.01	4.30 ± 0.99	2.0 ± 0.3	1.5	3–12.5	1.8–3.1
		Fe	4.2 ± 0.2	2.62 ± 0.01	12.85 ± 1.63				
	post-PROX	Pt	6.1 ± 0.2	2.72 ± 0.01	8.19 ± 1.25	6.5 ± 1.0	1.3	3–12.5	1.7–3.1
		Fe	1.8 ± 0.1	2.64 ± 0.01	9.05 ± 3.11				

[a]After treatment in H_2 flow for 1 h after O_2 flow for 1 h at 500 °C.
[b]After PROX experiment in 1%CO, 0.5%O_2, H_2 balance flow for 1 h at 200 °C.
[c]k range for Fourier transformation.
[d]Fitting range in R-space.

by Exner et al. in their TG–MS measurement for ion-exchanged platinum tetrammine complex on faujasaite X [13].

3.2. Exafs analyses

Figure 2 shows the k^3-weighted EXAFS functions and Fourier transformed them of Pt L_{III} and Fe K edge

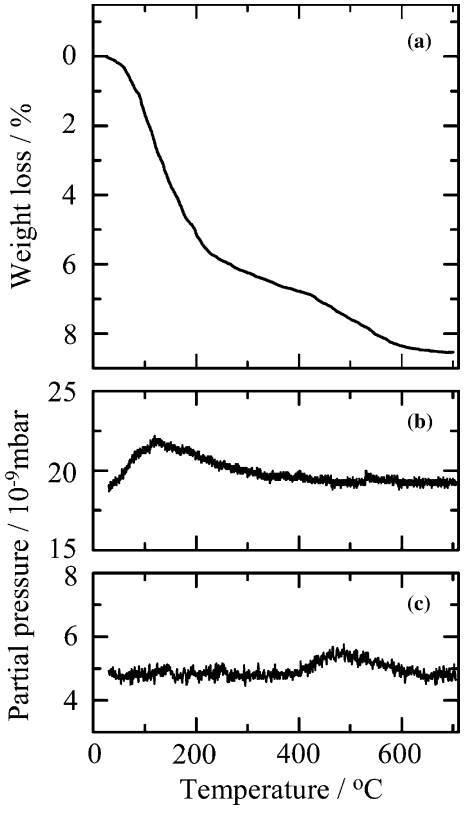

Figure 1. TG–MS profiles of ion-exchanged Pt–Fe(2:1)/M. (a) TG curve, (b) MS profile of $M/Z = 18$, (c) MS profile of $M/Z = 17$.

of H_2 pre-treated Pt–Fe(2:1)/M. In each EXAFS functions, S/N ratio is large enough up to 12 Å^{-1} for Pt L_{III} edge and 10 Å^{-1} for Fe K edge.

Fitting results on Pt–Fe(2:1)/M of ion-exchanged, H_2 pre-treated, and post-PROX are shown in table 1. As mentioned above, the fitting of Fe K and Pt L_{III} edge spectra was performed simultaneously. Unfortunately, Fe K edge data of other samples, i.e. Pt–Fe(3:1, 1:1)/M could not analyze due to the inferior quality of the data. Here, N, R, σ^2, ΔE and R_f are mean coordination number, inter-atomic distance, Debye–Wallar factor, energy shift and residual factor, respectively.

At the ion-exchanged catalyst, about four nitrogen atoms ($N_N = 3.9$) were coordinated to a centered Pt atom, but no evidences of the presence of coordinating Pt or Fe atoms were found. Consequently, this strongly supports the conclusion led by TG–MS measurements that Pt species were presumably supported in mordenite as $Pt(NH_3)_4$ with high dispersion after ion-exchange stage. On the other hand, Fe center atom is coordinated with Fe [$N_{Fe}(4.7)$] and oxygen [$N_O(5.0)$], indicating that Fe elements are loaded as oxide clusters, separated from the ion-exchanged $Pt(NH_3)_4$.

For the H_2 pre-treated catalyst (reduced in H_2 at 500 °C), Pt center atom is coordinated by Pt and Fe with increased numbers of $N_{Pt}(2.1)$ and $N_{Fe}(4.6)$, indicating the formation of Pt–Fe alloy clusters. Fe center atom is coordinated by not only Pt and Fe but also O even after H_2 reduction.

At the post-PROX catalyst, a dramatic reduction of N_{Fe} to Pt center atom is observed, i.e., from 4.6 to 1.9, accompanied with increase of N_{Pt} (from 2.1 to 6.4) to Pt center atom. For Fe center atom, an increase in oxygen coordination number N_O (from 2.6 to 4.3) and a disappearance of neighboring Fe ($N_{Fe} = 0$) are seen. These results immediately make us imagine that a major part of

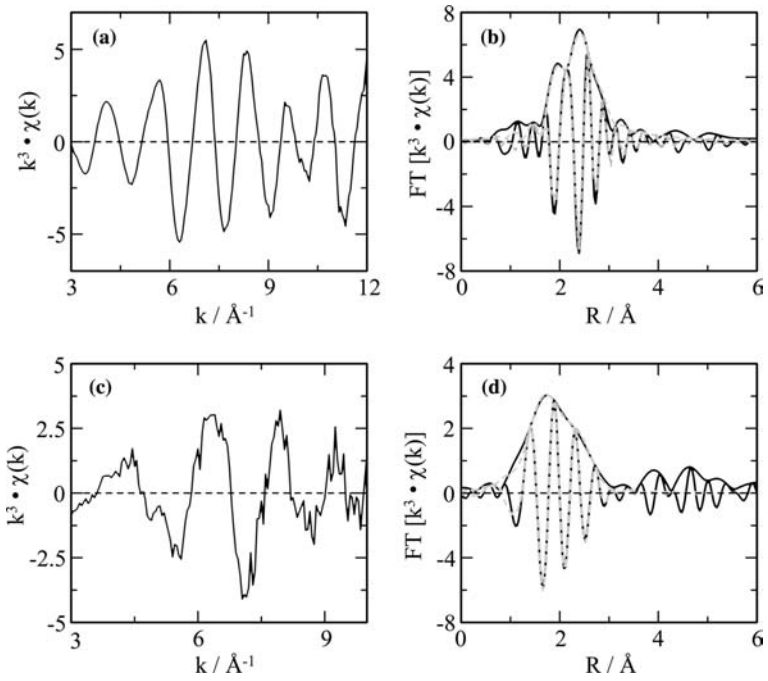

Figure 2. Extraction and Fourier transformation of k^3-weighted EXAFS function of Pt L_{III} and Fe K edge of H_2 pre-treated Pt–Fe(2:1)/M (a), (c) Extracted EXAFS function from Pt L_{III} and Fe K edge XAS spectra, respectively, (b), (d) Fourier transformation of their EXAFS functions, respectively (solid lines), with their curve fitting results (dotted lines).

Fe atoms on Pt–Fe clusters reacted with O_2 contained in the reactant flow, formed Fe oxides and probably stayed on Pt–Fe cluster surfaces during the PROX condition.

The results of EXAFS analysis on Pt–Fe(3:1, 2:1, 1:1)/M samples are compared in table 2. At the H_2 pre-treated catalysts, the Pt center atom was coordinated by both Pt and Fe at every catalyst, indicating the formation of Pt–Fe alloy. At the post-PROX samples, all of the coordination numbers for Pt converged at ca. 8 and was not increased further. In our previous work [9], we confirmed from STEM images of Pt–Fe(2:1)/M catalyst that 80% metal particles located inside mordenite pores, and only 20% outside the pores. The former particles were observed as images of about 1 nm diameter. Supposing the coordination number of the latter to be the maximum 12, the number of the residual 80% particles was calculated to be 7. The particles size calculated from this coordination number is about 1 nm [14], that agrees well with the value observed by STEM images. The metal particle size is a little larger than the mordenite pore size, i.e., 0.70 nm [15]. As the reason of the large particle size estimated, we can consider an underestimation of the percentage for the particles located outside of pores. The upper limit of the coordination number for the particles inside of pores must be controlled by the mordenite cage size. Thus, we concluded a major part of metal particles to be supported in mordenite cages.

3.3. Xanes analysis

Figure 3 shows XANES at Pt L_{III} edges for Pt–Fe(3:1, 2:1, 1:1)/M samples in the different treatment stages, referred to those of Pt metal foil and PtO_2. As seen in figure 3a, Pt edge position at the ion-exchanged Pt–Fe/M is seen between Pt foil and PtO_2 edges, indicating a charged state. Although the Pt valences can't be confirmed by itself, we may suggest it to be $Pt(NH_3)_4^{2+}$, since we used $Pt(II)(NH_3)_4Cl_2$ as the Pt source and also TG–MS and EXAFS indicated the Pt species to be supported in mordenite as $Pt(NH_3)_4^{n+}$ as mentioned above.

At H_2 pre-treated catalysts (see figure 3b), Pt edge positions of all Pt–Fe/M catalysts almost coincide with that of Pt foil, and only a slight positive shift can be seen. It is obvious, therefore, that Pt atoms on Pt and/or Pt–Fe clusters in the mordenite pores are mostly in no-charged metallic state after reducing with pure H_2.

After PROX treatment (see figure 3c), no noticeable shifts of Pt edge position from Pt foil are observed at Pt–Fe(3:1, 1:1)/M. However, it is to be noted that the Pt L_{III} edge energy for the most active catalyst, Pt–Fe(2:1)/M, shifts to a higher energy, while the white line intensity did not increase significantly. The explanation for this phenomenon is not clear at moment, but the shift in the edge position may be related to a core level shift, while the intensity of the white line is sensitive to the number of d-holes. Enhanced CO adsorption but not H_2 on Pt sites may be brought by the large core level shift, resulting in the superior selectivity on Pt–Fe(2:1)/M. This possibility is supported by a literature [16] showing the relationship between the surface core level shift and CO-Pt bonding energy at Pt catalyst.

Then, we carried out Fe K edge XANES measurement for check of the Fe state in Pt–Fe(2:1)/M of the

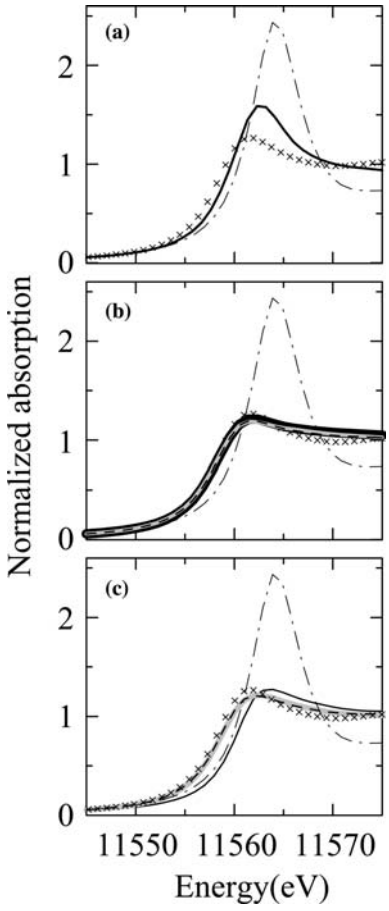

Figure 3. Pt L_{III} edge XANES spectra of various Pt–Fe/M catalysts and the reference samples: (a) ion-exchanged, (b) H_2 pre-treated, (c) post-PROX Pt–Fe(3:1)/M, Pt–Fe(2:1)/M, Pt–Fe(1:1)/M, ××× Pt foil, PtO_2.

different treatment stages mentioned above. Results are shown in figure 4 in comparison with references of Fe metallic foil, FeO and Fe_2O_3. As shown in figure 4a, the K edge of ion-exchanged Pt–Fe(2:1)/M coincides well with that of Fe_2O_3 edge, exhibiting that Fe exists as Fe^{3+}. This conclusion agrees well with the EXAFS result, mentioned above, as well as the fact using $Fe(NO_3)_3$ as Fe source in the catalyst preparation process.

H_2 pre-treated Pt–Fe(2:1)/M does not show a shoulder peak characteristic of the metallic Fe foil but rather resembles FeO as shown in figure 4b. Combining this observation and the above discussion on EXAFS, we can consider that the Fe state was reduced from Fe^{3+} to Fe^{2+} by H_2 treatment on Pt–Fe or Fe clusters and that Fe sites have oxygen atoms in adsorbed state or oxide state of FeO.

After PROX treatment at Pt–Fe(2:1)/M (see figure 4c), Fe edge position shows a positive shift toward the energy between FeO and Fe_2O_3. The ratio of Fe^{2+} to Fe^{3+} is estimated 0.75/0.25 by linear-combination-fitting the reference compounds spectra into the sample spectrum. The result indicates that Fe supported on mordenite is in more positively charged state between Fe^{2+} and Fe^{3+}, agreeing well with the EXAFS analysis, i.e., the noticeable reduction of N_{Fe} to Pt center atom and the contrary increase of N_O to Fe center atom in comparison with those of H_2 pre-treated sample.

FT-IR spectra of Pt(6 wt%)/M and Pt–Fe(2:1)/M are shown in figure 5, obtained at 30 °C and 200 °C in 1%CO/H_2 flow. At Pt/M, a major IR band appeared at 2077 cm^{-1} regardless the measuring temperatures, which can be assigned to the stretching band for the CO adsorbed on Pt sites [17]. This band was also observed at Pt–Fe(2:1)/M, although the amount of CO adsorbed on Pt sites reduced, especially at 200 °C. $Fe(CO)_5$ vapor gives two infrared bands at 2034 and 2012 cm^{-1} [18] and IR bands of CO adsorbed on Fe film deposited on Cu(111) appear at 2032 and 2000 cm^{-1} [19]. At Pt–Fe(2:1)/M, no noticeable bands, which should be assigned to such a CO-Fe bonding, can be observed in figure 5. Thus, we can conclude that CO adsorption occurs preferentially on Pt sites on Pt–Fe(2:1)/M catalyst, and that Fe sites, which are in oxide states as shown by EXAFS and XANES, have very poor affinity to CO adsorption. After N_2 purge, the band of Pt/M shows almost no change. On the other hand, the small CO-Pt band ats Pt–Fe/M disappeared not only at 200 °C but also 30 °C. Therefore, it is clear that the presence of Fe or its oxide near Pt sites suppress not only the CO

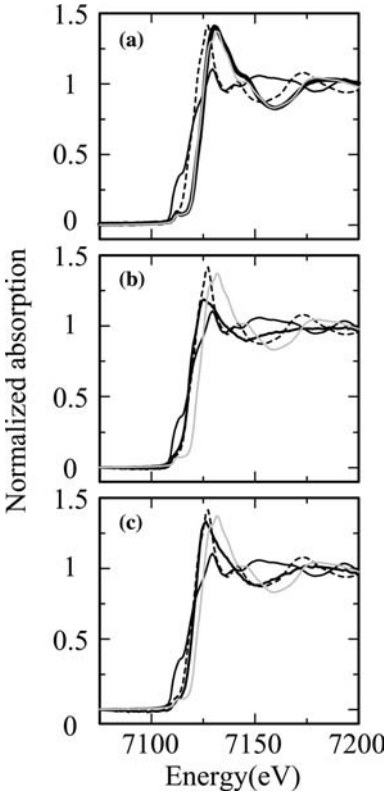

Figure 4. Fe K edge XANES spectra of Pt–Fe(2:1)/M catalyst and the reference samples: (a) ion-exchanged, (b) H_2 pre-treated, (c) post-PROX Pt–Fe(2:1)/M, Fe foil, FeO, Fe_2O_3.

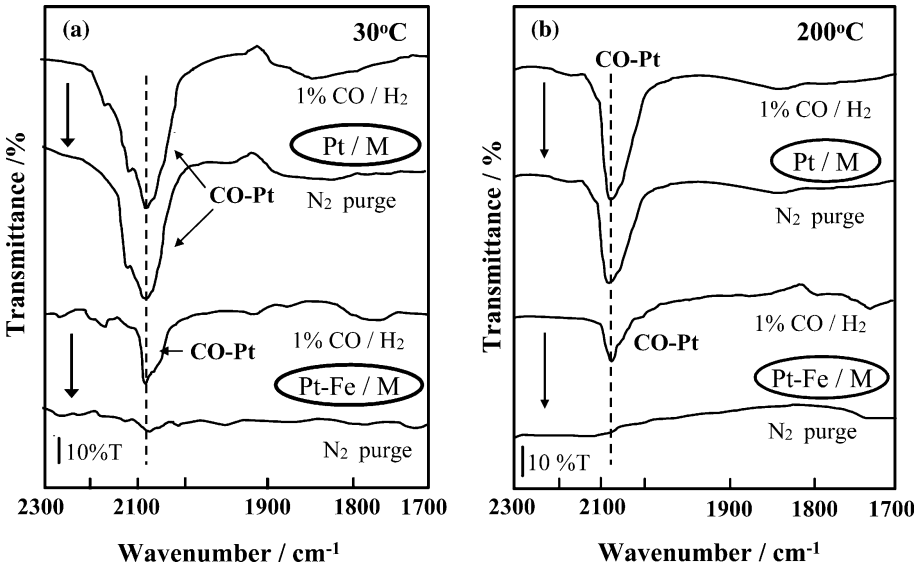

Figure 5. FTIR spectra at Pt(6wt%)/M and Pt–Fe(2:1)/M after flowing 1%CO/H_2 and N_2 for 15 min, respectively, at different temperatures; (a) 30 °C, (b) 200 °C.

coverage but also the bond strength at Pt sites. Corresponding behavior to the present observation has been found by Watanabe et al. at Pt–Fe alloy and the similar ones for the CO tolerant H_2 electrooxidation at fuel cell anodes, where CO coverage on Pt sites was suppressed less than 0.5 under the steady-state operation, see, e.g., refs. [20, 21]. They ascribed the phenomena to the increase of Pt 5d-vacancy by alloying with non-precious metals of such transient metals as Fe, Ni, Co etc.

From these results, we can conclude about the mechanism of the enhanced PROX at Pt–Fe/M as in the following manner. At Pt/Al_2O_3, CO adsorption to Pt occurred predominantly at low temperature and it blocked O_2 and H_2 adsorption [22]. At our Pt/M, CO adsorption was still strong even at 200 °C, as shown in figure 5, resulting in the low PROX performance below 150 °C [9]. However, in the case of Pt–Fe/M, Pt sites adsorb weakly bonded CO molecules and Fe sites adsorb oxygen, as seen above. Consequently, Fe and Pt sites adjacent each other play rules of adsorption sites for oxygen and CO, respectively, and can enhance the following surface reaction between them. Pt L_{III} edge shift was observed only at Pt–Fe(2:1)/M, which has the highest PROX activity. It is presumed this edge shift may be related deeply to the highest PROX activity. Investigations about the detail relationship between this edge-shift and the PROX activity are going on and will be reported elsewhere.

4. Conclusion

In order to understand the superior PROX performance of Pt–Fe/M catalysts and the maximum performance at Pt–Fe(2:1)/M, we performed XAFS and FTIR measurements. The results showed that Pt sites act as CO adsorption sites and Fe sites behave as the oxygen adsorption sites even under H_2 containing atmosphere. Pt in Pt–Fe(2:1)/M shows Pt L_{III} edge shift different from the other composition catalysts during the PROX reaction. Therefore, this edge-shift and the PROX activity may be related deeply each other. Based on the above results, we explained the superior PROX property at the Pt–Fe/M and proposed the enhanced mechanism.

References

[1] R.A. Lemons, J. Power Sources 29 (1990) 251.
[2] H. Igarashi, T. Fujino and M. Watanabe, J. Electroanal. Chem. 391 (1995) 119.
[3] M. Watanabe and S. Motoo, J. Electroanal. Chem. 60 (1975) 275.
[4] M.L. Brown Jr. and A.W. Green, Ind. Eng. Chem. 52 (1960) 841.
[5] P.V. Snytnikov, V.A. Sobyanin, V.D. Belyaev, P.G. Tsyrulnikov, N.B. Shitova and D.A. Shlyapin, Appl. Catal. A 239 (2003) 149.
[6] M. Watanabe, H. Uchida, H. Igarashi and M. Suzuki, Chem. Lett. (1995) 21.
[7] H. Igarashi, H. Uchida and M. Watanabe, Chem. Lett. (2000) 1262.
[8] H. Igarashi, H. Uchida and M. Watanabe, Stud. Surf. Catal. 132 (2001) 953.
[9] M. Watanabe, H. Uchida, K. Ohkubo and H. Igarashi, Appl. Catal. B 46 (2003) 595.
[10] M. Newville, P. Livins, Y. Yacoby, E.A. Stern and J.J. Rehr, Phys. Rev. B 47 (1993) 14126.
[11] M. Newville, B. Ravel, D. Haskel, J.J. Rehr, E.A. Stern and Y. Yacoby, Physica B208-209 (1995) 154.
[12] A.L. Ankudinov, B. Ravel, J.J. Rehr and S.D. Conradson, Phys. Rev. B 58 (1998) 7565.
[13] D. Exner, N. Jaeger, K. Moller and G. Schulz-Ekloff, J. Chem. Soc. Faraday Trans. 1 78 (1982) 3537.
[14] J. de Graaf, A.J. van Dillen, K.P. de Jong and D.C. Koningsberger, J. Catal. 203 (2001) 307.

[15] W.M. Meier, Z. Kristallogr. 115 (1961) 439.
[16] G.F. Cabeza, P. Legare and N.J. Castellani, Surf. Sci. 465 (2000) 286.
[17] P. Pillonel, S. Derrouiche, A. Bourane, F. Gaillard, P. Vernoux and D. Bianchi, Appl. Catal. A 278 (2005) 223.
[18] R. Cataliotti, A. Foffani and L. Marchetti, Inorg. Chem. 10 (1971) 1594.
[19] T. Tanabe, R. Buckmaster, T. Ishibashi, T. Wadayama and A. Hatta, Surf. Sci. 472 (2001) 1.
[20] M. Watanabe, H. Igarashi and T. Fujino, Electrochemistry 67 (1999) 1194.
[21] H. Igarashi, T. Fujino, Y. Zhu, H. Uchida and M. Watanabe, Phys. Chem. Chem. Phys. 3 (2001) 306.
[22] S.H. Oh and R.M. Sinkevitch, J. Catal. 142 (1993) 254.